Performance and durability of pure-water-fed anion-exchange-membrane electrolyzers using baseline materials and operation

Grace A. Lindquist,[†] Sebastian Z. Oener,[†‡] Raina Krivina,[†] Andrew R. Motz,[ǂ] Alex Keane, [ǂ]

Christopher Capuano, [ǂ] Katherine E. Ayers, [ǂ] and Shannon W. Boettcher,*[†]

[†]Department of Chemistry and Biochemistry and the Oregon Center for Electrochemistry, University of Oregon, Eugene, Oregon 97403

[‡]Present: Department of Interface Science, Fritz-Haber Institute of the Max Planck Society, Berlin, Germany

[ǂ]Nel Hydrogen, Wallingford, Connecticut 06492

* swb@uoregon.edu

Keywords: water electrolysis, membrane electrolysis, anion exchange membrane, ionomer stability, membrane conditioning

Abstract

Water electrolysis powered by renewable electricity produces green hydrogen and oxygen gas, which can be used for energy, fertilizer, and industrial applications and thus displace fossil fuels. Pure-water anion-exchange-membrane (AEM) electrolyzers in principle offer the advantages of commercialized proton-exchange-membrane systems (high current density, low cross over, output gas compression, etc.) while enabling the use of less-expensive steel components and non-precious-metal catalysts. AEM electrolyzer research and development, however, has been limited by the lack of broadly accessible materials that provide consistent cell performance, making it difficult to compare results across studies. Further, even when the same materials are used, different pretreatments and electrochemical analysis techniques can produce different results. Here, we report an AEM electrolyzer comprised of commercially-available catalysts, membrane, ionomer, and gas-diffusion layers operating near 1.9 V at 1 $A \cdot cm^{-2}$ in pure water. After initial break in, the performance degraded by 0.67 $mV \cdot h^{-1}$ at 0.5 $A \cdot cm^{-2}$ at 55 °C. We detail the key preparation, assembly, and operation techniques employed and show further performance improvements using advanced materials as a proof-of-concept for future AEM-electrolyzer development. The data thus provides an easily reproducible and comparatively high-performance baseline that can be used by other laboratories to calibrate the performance of improved cell components, non-precious metal oxygen evolution and hydrogen evolution catalysts, and learn how to mitigate degradation pathways.

Introduction

Hydrogen gas is used as a feedstock for vital industrial processes including ammonia-based fertilizer production, metal-ore refining, and chemical production.[1] It is also of significant interest

for energy storage and transportation,[2] and central in plans for reducing, and eventually eliminating, CO_2 emissions.[3-4] Such technology, however, is only 'green' if powered using renewably-produced hydrogen, for example, through water electrolysis powered by wind or solar. Of the 70 Mt (megatons) of hydrogen used globally each year, only ~1% is produced through electrolysis.[5] The rest is essentially all produced from fossil fuels by coal gasification and natural-gas reforming and contributes more than 830 Mt of CO_2 emissions annually.[5]

To achieve the electrolyzer capacity required to meet global hydrogen demands, both capital and operating costs must decrease.[6] The best technology for this scale up is not yet evident. While low-temperature liquid-alkaline and proton-exchange-membrane (PEM) electrolyzers are mature, anion-exchange-membrane (AEM) electrolyzer technology is still under development.[7] The largest limitations of AEM systems have been membrane and ionomer conductivity and stability. Increasing the ionic conductivity of an AEM usually also increases its solubility and water uptake,[8-10] thus ionic conductivity is often sacrificed to achieve the required mechanical durability for electrolyzer hardware. Commercial PEM electrolyzers operate in pure water at 1.8 - 2 V at 1.5 - 2 $A \cdot cm^{-2}$ for thousands of hours, with optimized lab-scale devices achieving similar voltages at higher current densities.[11] Most reported AEM electrolyzers operate in carbonate- or hydroxide-based electrolyte that mask the stability issues of the ionomer in the alkaline oxidative environment. Many previous AEM electrolyzers running in dilute electrolyte or pure water typically have limited durability and at 2 V provide only a few hundred $mA \cdot cm^{-2}$.[12-15]

Recent work has shown more-competitive AEM performance in pure water, achieving cell potentials below 2 V at 1 $A \cdot cm^{-2}$.[16-18] These studies use custom-made membrane and ionomer materials[16-17] and/or specialized gas diffusion layers (GDLs).[18] Testing protocols have also involved operation in alkaline electrolyte prior to pure water testing.[16-17] Residual electrolyte may

affect performance and also introduces uncertainty regarding degradation mechanisms associated with the ionomer relative to performance loss due to flushing supporting electrolyte (see additional discussion and data below in the context of the experiments reported here). Without widely available materials and defined testing protocols, it is difficult to reproduce performance and the field is not accessible to the broader research community.

A significant limitation facing AEM research is the lack of consistent, high-performing, stable baseline materials. Standard PEM systems use Nafion as the membrane and ionomer binder, a Pt black/Toray carbon-paper cathode, and IrO_2/Ti anode.[19] No such baseline materials exist for AEM systems and a wide variety of membranes, ionomers, catalysts, and gas diffusion layers (GDLs) are used.[12-14] This impediment is exemplified in the surge of earth-abundant oxygen- and hydrogen-evolution-catalyst research reporting AEM electrolyzer polarization curves obtained under conditions that are not always well defined and often irrelevant to practical applications, and/or with older membrane chemistries. The use of the AEM-GDL interface in new fields, such as for bipolar membranes,[20-22] could lead to similar problems. The complexity of membrane electrolyzers requires interdisciplinary efforts that leverage baseline materials and well-defined conditions to compare results across studies.

While materials play a significant role in determining MEA performance and stability, preparation and assembly technique, as well as electrochemical analysis procedure, are also crucial. Different coating techniques (e.g. airbrush versus hot-press, or coated membranes versus coated GDLs) result in different interactions between the catalyst, ionomer binder, and membrane at the triple-phase boundary. Therefore, large performance differences can be observed across MEAs of identical materials.[23] During electrolyzer operation, different electrolyte pre-treatments have also been used, even if testing in pure water,[16-17, 24] which can also affect measured

electrolyzer performance and durability. Here, we detail the preparation and operation of an inexpensive small 1 cm^2 AEM electrolyzer operating with pure water below 2 V at 1 $A \cdot cm^{-2}$ using commercially-available materials. These commercial stainless-steel GDLs (original designed as filter media) have a graded porosity, a property which has been previously shown in custom materials to be useful for optimizing membrane-electrolyzer performance.[25-27] We use an inexpensive hand-held spray-coating gun, instead of a commercial spray-coater, making the approach more widely accessible. The quality of the interface was found to be key for improved durability. Through initial optimization, we show improved durability reported in pure water at 0.5 $A \cdot cm^{-2}$ with the baseline material compared to other available systems, and reveal insight into initial degradation pathways. We also show the importance of sufficient pure-water purging of the system if electrolyte pre-treatments are used. This baseline MEA configuration, along with baseline fabrication and testing procedures, can be used as a starting reference for further AEM materials development.

Experimental Methods

Catalyst dispersions and GDL coating. Pt black (high surface area, Fuel Cell Store) and IrO_2 (Pajarito Powder) nanoparticles were used as the cathode and anode catalyst, respectively. Cathode and anode ink solutions were prepared identically. For every 100 mg of catalyst, 0.5 g H_2O was added, followed by 1.7 g of 2-propanol. The PiperION (TP-85, 5% w/w in ethanol), Sustainion (XB-7 5% in ethanol), and Aemion (AP1-HNN8-00-X) ionomer solutions were used with the corresponding membrane. The Aemion ionomer solid was dissolved in ethanol to yield a 5% w/w solution before ink preparation. Ionomer solution (200 mg of 5% solution in ethanol) was added

to yield the final 10 wt. % ($w_{ionomer}/w_{catalyst}$) ink. Inks were then bath-sonicated (Branson 1510R-MTH) at room temperature for a minimum of 1 h (Pt black) or 2 h (IrO_2) until fully dispersed.

Toray 090 carbon paper (Fuel Cell Store) and a stainless-steel mesh filter material (25AL3, Bekaert) were used as the cathode and anode GDLs, respectively. The GDL was taped to a hot plate set to 80 ºC. Catalyst inks were sprayed onto the GDL materials using an airbrush (Testors, Aztek A2203, part of the Amazing Airbrush kit) and compressed N_2 at a pressure of 12 psi. A catalyst loading between 2.3 and 2.8 mg·cm^{-2} was determined by mass difference. A thin layer (1-2 wt. % $w_{ionomer}/w_{catalyst}$) of ionomer solution in ethanol was sprayed on top of the catalyst layer to improve contact with the membrane. As the quality of the catalyst ink layer has a significant effect on the overall MEA performance, particular attention and care should be paid to the GDL airbrush coating technique. Specific details describing the electrode preparation are included in the Supplemental Information.

Membrane conditioning. PiperION (TP-85 50 μm and 40 μm, W7Energy), Sustainion (X37-50, Dioxide Materials), and Aemion (AF1-HNN8-50-X, Ionomr) membranes were conditioned according to manufacturer instructions. The membranes were soaked in 0.5 M KOH (PiperION), 1 M KOH (Sustainion), or 3 M KOH (Aemion) for 48 h, replacing the solution with fresh KOH after 24 h. Membranes were stored in their respective KOH solution when not in use. The thickness of hydrated membranes was determined by clamping each membrane between two glass slides and measuring the thickness using a Keyence VHX 7000 digital microscope.

MEA assembly. The serpentine flow fields can apply an uneven pressure to the relatively flexible SS GDL, so a sintered Ti plate was used as a rigid back support on both the cathode and anode side (400 μm thickness, Baoji Yingao Metal Materials Inc.). Gasket material (0.005" PET/PETE clear film, McMaster-Carr) was laser cut to an active area of 1 cm^2. Gaskets were

added until they were flush with the GDL surface. The number of gaskets was determined by adding/removing a gasket until maximum performance was obtained. For this cell, this was determined to be seven total gaskets at the anode and six at the cathode. The Sustainion membrane required one additional gasket at each electrode to prevent the membrane from tearing. The conditioned membrane was dipped in a beaker of 18.2 MΩ·cm water then rinsed with 18.2 MΩ·cm water for 10 s before assembly. Materials were assembled in the stack and a torque wrench was used to tighten the screws to 5.6 Nm.

Electrolyzer operation. 18.2 MΩ·cm water (or in certain experiments 1 M KOH) was flowed to the cathode and anode at 500 $mL \cdot min^{-1}$. N_2 was bubbled into the water tank. The anode water flow (carrying produced O_2) was recirculated in the system while the cathode water flow (carrying produced H_2) was flowed into a chemical hood, degassed with N_2, then recirculated back into the water tank. Temperature was maintained at the specified value and was monitored with a thermocouple inserted into the cell hardware (Fig. S2). Once the cell temperature was stable, the MEA was conditioned by stepping the current from 100 $mA \cdot cm^2$ to 1 $A \cdot cm^{-2}$, holding for 2 min at each step. The cell was then held at 1 V to test for pinholes or other short-circuit pathways in the cell (the steady sate electrolysis current decays to zero at < 1.23 V, while shunt currents persist). The cell was brought back to 1 $A \cdot cm^{-2}$ for 2 min to stabilize. The potential was then recorded, and the current was decreased in 100 $mA \cdot cm^{-2}$ steps measuring the potential for 10 s at each step to collect the JV curve. The cell was held at 500 $mA \cdot cm^{-2}$ for stability measurements. Linear sweep voltammetry (LSV) measurements were collected from 1.3 - 2 V at a scan rate of 20 $mV \cdot s^{-1}$. A full detail of all relevant materials and parameters is given in Fig. 1 and the Supplemental Information.

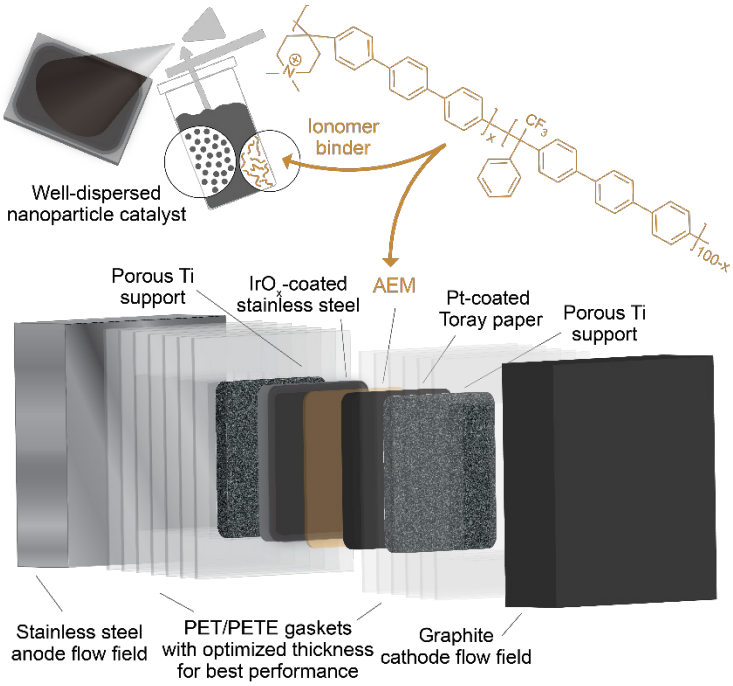

Figure 1: Schematic detailing the preparation and assembly of the 1-cm^2 MEA. The small cell size allows for rapid and economical studies of different parameters as well as degradation phenomena, even with a standard potentiostat station. The example here is using the PiperION membrane and ionomer, and the same process was used for the Aemion and Sustainion membranes/ionomers.

Additional analysis. After operation, the electrolyzer membrane electrode assembly (MEA) was disassembled with the anode and cathode GDLs peeled off the membrane. The anode GDL with remaining IrO_x and PiperION ionomer was dried at room temperature for 48 h and analyzed with X-ray photoelectron spectroscopy (XPS) on an ESCALAB 250 (ThermoScientific) using an Al Kα monochromated (20 eV pass energy, 500 μm spot size) source. The samples were charge-neutralized using an in-lens electron source. Spectra were analyzed using ThermoScientific Avantage 4.88 software. The C 1s signal at 284.8 eV was used to calibrate the binding energy scale. The spectra then was compared to the spectra of a pristine PiperION thin film spin-coated from the the 5 wt% ionomer solution onto an Au-coated glass slide.

Results and Discussion

Table 1. Membrane properties

Membrane	Aemion	Sustainion	PiperION
Ion exchange capacity ($meq \cdot g^{-1}$)	2.1-2.5	1.1	2.02-2.37
Reported OH^- conductivity ($mS\ cm^{-1}$)	>80, no specified temperature	>130* at 70 °C	>135 at 70 °C
Reported % water uptake	33-37%	80%	50%
Dry thickness (μm)**	50	50	50
Wet thickness*** (in KOH, μm)	73	72	62
Chemical structure (including manufacturer-provided counter ion)	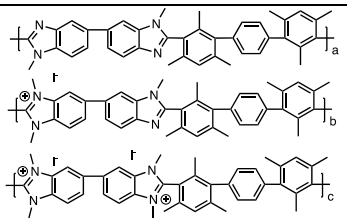	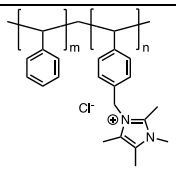	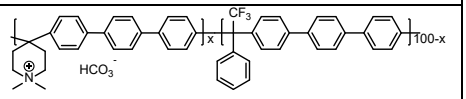
Ref.	28	29	30

*Reported conductivity is calculated from area-specific resistance (ASR) in 1 M KOH at 60 °C. While Sustainion has a lower IEC, the higher water uptake has been reported to result in a lower ASR leading to the comparable OH^- conductivity value. ** The membranes studied here were all selected because they are commercially available and thus easily accessible. The common thickness for each membrane was 50 um, so this thickness was chosen to keep this parameter constant across all experiments. ***See Fig. S3 for measurement images.

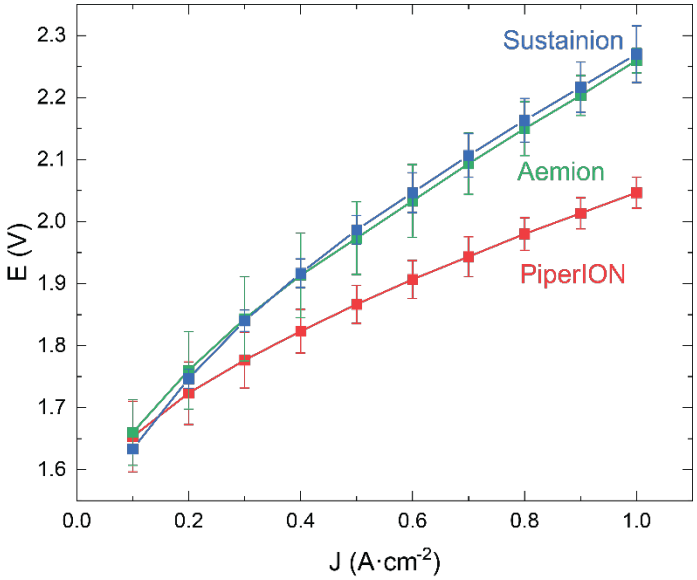

Figure 2: Performance comparison of electrolyzers from three commercially-available AEMs. All experiments were run with pure water at a cell temperature of 55 ± 1 °C. All membranes are 50 μm thick. Each curve is the average of three individual MEA's tested. Error bars are the standard deviation obtained from 3 separately fabricated devices.

The performance of Aemion, Sustainion, and PiperION AEM electrolyzers are shown in Fig. 2. All tests were operated at the same temperature (55 ± 1 °C). It should be noted each membrane/ionomer system requires optimized ionomer loading for best performance, which may be different for each system. Here ionomer content was not optimized to any specific membrane, but rather 10 wt% ionomer was chosen to maintain continuity across all membranes. The temperature selected was the highest temperature the Aemion membrane was able to withstand, based on the reported maximum operating temperature of the Aemion membrane. For further validation, the Aemion membrane was operated at 69 ± 1 °C and a rapid performance degradation was observed (Fig. S4). At 100 $mA \cdot cm^{-2}$, membrane resistance and mass transport effects do not substantially contribute to voltage losses and all membranes show nearly identical performance. As current density increases Aemion and Sustainion continue performing similarly, while PiperION out-performs both. The lower hydroxide conductivity of Aemion is likely contributing to its higher voltage performance, specifically at the catalyst interface. Lower hydroxide-ion conductivity is particularly detrimental at the reactive electrode interfaces[31] where it may lead to larger voltage losses than expected from simple ionic membrane-series-resistance arguments. It should be noted the hydroxide exchange process was found to have a strong impact on Aemion performance (Fig. S5). Each membrane arrives with different counter ions (Table 1) which are exchanged for OH^- before electrolyzer operation. Weakly-hydrated ions interact more strongly with the charged end-groups of the AEM[32] and thus require higher concentrations of hydroxide for ion exchange and can be incompletely exchanged. MEA performance is also dependent on the applied hardware pressure;[33] the increased resistance observed with Sustainion might be in part due to the additional gasket material required for Sustainion operation resulting in a higher resistance due to non-ideal or non-uniform cell compression.

The temperature dependence of the PiperION membrane was further investigated (Fig. 3). While some AEMs are not stable at elevated temperatures,[34] the PiperION membrane operated well at all temperatures tested, and has been reported operating up to 90 °C.[18] The voltage decreases with increasing temperature due to increasing membrane/ionomer OH^- conductivity and improved reaction kinetics.

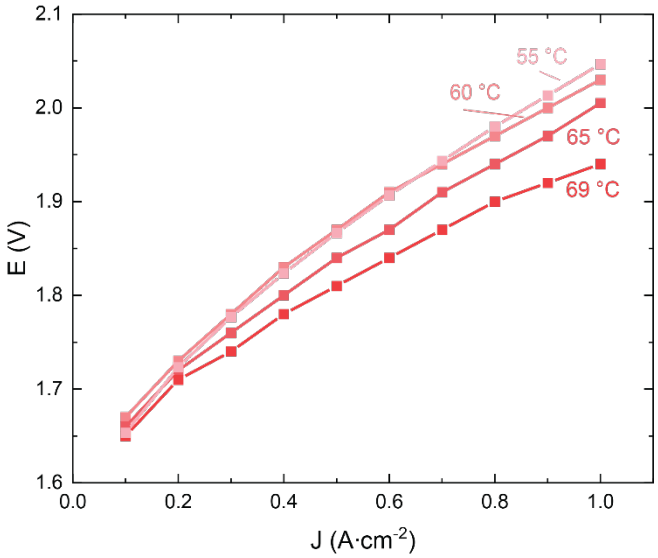

Figure 3: Temperature dependence of an electrolyzer operated in pure water with the 50-um-thick PiperION MEA.

Various cell conditioning methods were then compared for the PiperION system. Cell conditioning is a well-established practice for PEM electrolyzers and fuel cells,[35-36] during which the cell is operated and performance gradually improves.[37] While the detailed processes that cause this improvement are not fully understood, it is hypothesized that cell conditioning further activates catalyst surfaces, more-fully hydrates the membrane and ionomer, and better establishes ion pathways through the membrane and ionomer.[36, 38-39] In this system, the cell is conditioned in pure water by applying current from 100 mA·cm^{-2} to 1 A·cm^{-2} in 100 mA steps holding for 2 min at each step. After conditioning, the cell was stepped from 1 A·cm^{-2} to 100 mA·cm^{-2} in 100 mA

steps holding for 20 s at each step. There is a notable difference in the time required for the voltage to reach steady state, as observed in Fig. 4a and b. The polarization curves obtained during and after cell conditioning (from Fig. 4a and b) were compared by plotting the voltage at 2 min and 20 s, respectively (Fig. 4c). As is shown, there is a significant difference in low-current-density performance before and after this initial conditioning period. This highlights the importance of sufficient cell conditioning prior to data collection.

Another commonly used process for pure-water AEM electrolyzer operation is to condition the cell in alkaline electrolyte, purge the cell with pure water, then measure the performance.[16-17] We compared this method to that used here. After conditioning and collecting a polarization curve using the current-step method, an LSV was collected at 20 $mV \cdot s^{-1}$ from 1.3 to 2 V. As can be seen, these results agree well, showing that after sufficient conditioning there is no significant difference in electrochemical technique used to collect the polarization curve. Next, 1 M KOH was flowed to both the cathode and anode and an LSV was collected. The full polarization curve in 1.0 M KOH up to 2 V resulting in ~ 4 $A \cdot cm^{-2}$ of current is included in Fig. S6. Then, pure water was returned to the cell, and an LSV was collected after 500 mL of water was purged through the system (following the procedure used by Li et al.).[16] The performance obtained using this method is significantly better than that obtained by conditioning in pure water. After collecting this LSV, the conductivity of the effluent electrolyte was measured over time. The effluent conductivity was still decreasing, even after > 1 L of pure water was flowed through the cell (Fig. S7), therefore this enhanced performance is attributed to residual KOH that was not sufficiently purged. After pure water was flowed for an additional 3 min (an additional 1.5 L of water) and the conductivity of the effluent was stable, four sequential polarization curves were collected (Fig. 4b). To stabilize the polarization curves, > 2.5 L of pure water was needed to flow through the small 1 cm^2 electrolyzer,

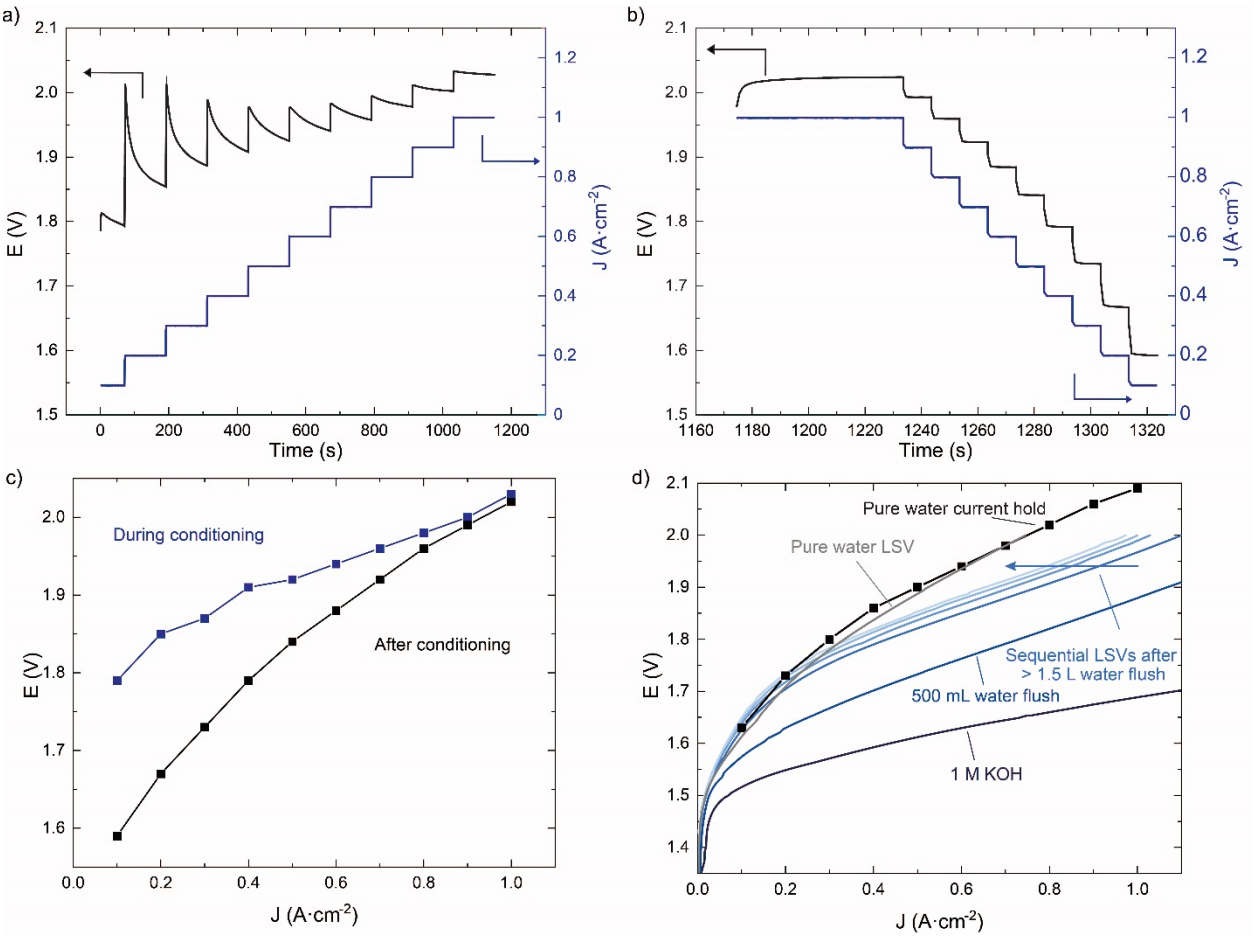

Figure 1: Effect of cell conditioning on polarization curves. Voltage changes over time when stepping current a) at cell start-up and b) after completing cell break-in. c) comparison of polarization curves collected during and after electrolyzer conditioning. d) comparison of polarization curves at various points when conditioning in 1 M KOH. All data was collected at 55 ± 1 °C with either a 50 µm thick (a-c) or 40-µm-thick (d) membrane.

yet the voltage was still lower than the recorded pure-water baseline (without KOH flow for pre-treatment). This result shows that performance enhancements from conditioning in hydroxide-containing electrolyte might not be completely attributed to residual OH^- in the system.

The residual performance increase after extensive pure water purging might be due to more-complete exchange of OH^-, for example due to removal of residual carbonate species in the ionomer or membrane that increases the ionic conductivity of the ionomer in the catalyst layer.[40] The lower swelling conditions of the conductive electrolyte might also create a more-favorable environment for the catalyst-ionomer interaction during conditioning. We note that all pure water

entering the electrolyzer was purged with N_2 while the KOH solution was not purged. While this effect is complex and requires further investigation, the results clearly show the importance of ensuring data is being collected in true pure-water conditions if using a conductive electrolyte for conditioning and that previously reported high-performance "pure-water" experiments are likely influenced by residual KOH.[16]

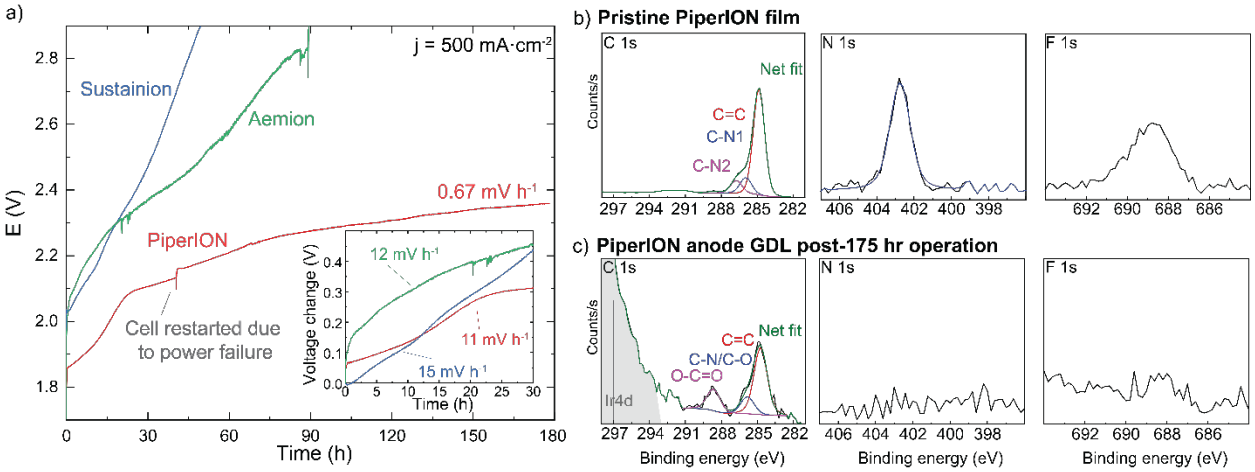

Figure 2: a) Stability comparison of the three commercial AEMs when operating at 500 mA·cm^{-2} at 55 °C in the electrolyzer. Experiments were ended when the total cell voltage exceeded 2.9 V. All membranes display a similar degradation rate for the first ~20 h (inset). b) XPS of a pristine PiperION film and c) PiperION anode GDL surface after 175 h of operation showing substantial evidence of oxidized carbon and loss of N and F.

The stability of each membrane was evaluated over 175 h of operation at 0.5 A·cm^{-2} (Fig. 5). Over the first ~20 h, all membranes show similar fast degradation rate of 11-15 mV·h^{-1} (Fig. 5 inset), indicating a similar degradation mechanism. After this initial "break-in" the PiperION system stabilizes. This MEA was continuously operated for over 175 h with a degradation rate of 0.67 mV·h^{-1} over the last 20 h. The Aemion and Sustainion systems were shut down when the cell voltage exceeded 2.9 V. While it is possible these systems stabilize in a similar manner to PiperION, the system voltage is too high for energy-efficient operation.

Membrane and ionomer degradation are complex processes that are still not fully understood, and there are potentially multiple different degradation pathways contributing.[41] The stability tests

were purposefully conducted at conditions that can be easily reproduced by other groups. To begin understanding the source of degradation of the PiperION system, after conditioning and operation in pure water, 1 M KOH was then flowed to the anode and cathode and the change in voltage observed (Fig. S8). After introducing electrolyte, the degradation rate increased from 24 $mV \cdot h^{-1}$ to 87 $mV \cdot h^{-1}$. Further, black particulates were observed in the cathode stream, indicating mechanical failure of the cathode. We hypothesize this is either attributed to the sudden increase in electrolyte conductivity shocking the cathode ionomer or a degradation mechanism influenced by the increasing hydroxide concentration or K^+ counter-ions, leading to breakdown and catalyst detachment. Such effects would not affect the durability during continuous pure water operation and therefore are not contributing to the observed degradation discussed previously. After, pure water was purged through the system for 10 min and then KOH was flowed only to the anode. After the pure-water purge (red line until 0.5 h in Fig. S8) the total voltage rapidly exceeds the previous values obtained during the initial pure water operation (black trace), indicating anode ionomer degradation, already during the pure water operation (black trace). Once KOH is flown to the anode (red trace after 0.5 h in Fig. S8) the degradation rate decreased from 96 $mV \cdot h^{-1}$ to 40 $mV \cdot h^{-1}$ (Fig. S8), suggesting that the increased conductivity with the KOH compensates for the loss in conductivity from the degrading ionomer.

To further investigate this degradation, the PiperION MEA was disassembled after 175 h steady-state operation and XPS was collected on the anode GDL surface which remained coated with catalyst and ionomer after disassembly (Fig. 5c). Additional C peaks associated with oxidized species along with a loss of F and N signal compared to a pristine PiperION film (Fig. 5b), demonstrating the ionomer in this region is undergoing significant oxidative damage. However,

more research is essential to understand the impact of oxidizing electrode potentials on the specific ionomers, among other effects such as CO_2 poisoning (and CO_3^{2-} formation).

The MEA described here is a starting baseline for further AEM materials development. Examples of improvements are shown in Fig. 6 using custom GDL and thinner membrane materials. The 40-µm-thick membrane shows ~100 mV improvement across all current densities. Proprietary Ti-based GDLs engineered to improve mass-transport and decrease system resistance for acidic PEM electrolyzers were obtained from Nel Hydrogen. When replacing the commercial stainless-steel GDLs with this material, a similar improvement of 90 mV is observed at 100 $mA \cdot cm^{-2}$, but only 30 mV at 1 $A \cdot cm^{-2}$ indicating resistive losses, likely in the catalyst/ionomer layers, are more important at high current densities. A lower resistance was observed with the 40-µm-thick membrane as indicated by the decreased slope. The improved performance might also be due to improved water management at the electrode interfaces creating and maintaining a better ionomer/catalyst interface.[9]

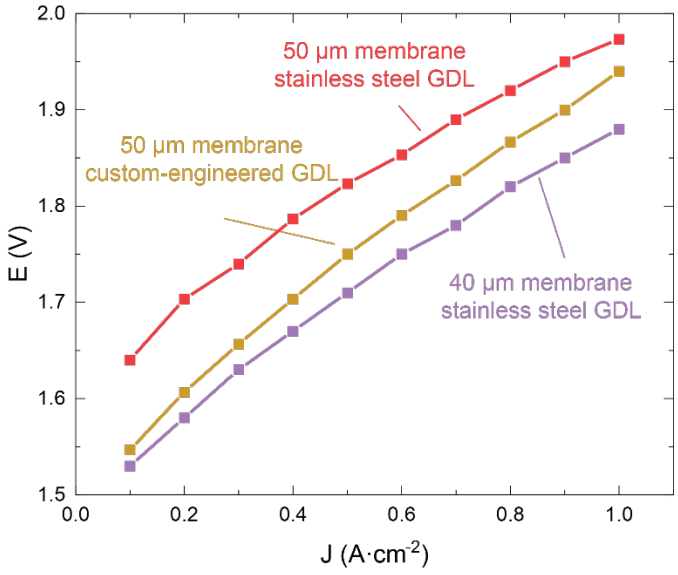

Figure 6: Improvements to baseline performance using enhanced materials. All cells were operated at 69 ± 1 °C. All cathode materials remained unchanged. The anode catalyst is IrO_2 on the designated GDL material.

Conclusion

We described the materials and preparation technique for baseline AEM pure-water electrolyzers with state-of-the-art performance and durability. The baseline AEM system performs below 2 V at 1 $A \cdot cm^{-2}$ and was tested for > 175 h reaching a final degradation rate below 1 $mV \cdot h^{-1}$ in pure water at 0.5 A cm^{-2}. We further demonstrated the importance of proper cell conditioning before data collection to ensure true pure-water performance is reported. All materials are commercially available and the cell size is small, making this performance an accessible baseline to the research community for further development. Operation using improved GDLs and a thinner membrane are shown as examples for future improvements. These examples highlight that improving OH^- conductivity, mass transport, and long-term ionomer stability are key issues for developing commercially relevant pure-water AEM electrolyzers.

Acknowledgements

This work was supported by the U.S. Department of Energy's Office of Energy Efficiency and Renewable Energy (EERE) under the Fuel Cell Technologies Office (FCTO) under award number DE-EE0008841. S.Z.O. acknowledges support from a research fellowship of the German Research Foundation (Deutsche Forschungsgemeinschaft) under project number 408246589 (OE 710/1-1). G.A.L. acknowledges Raina Krivina, Qiucheng Xu, and Lihaokun Chen for their valuable discussion.

Supporting Information. The Supporting Information is available free of charge at https://pubs.acs.org/doi/10.1021/acsami.XXXXX.

Additional materials preparation detail; electrolyzer hardware photos; digital microscope images of membrane cross sections; high temperature Aemion performance; effect of ion exchange on Aemion performance; PiperION performance in 1M KOH; effluent conductivity for KOH-spike measurements; cell stability in KOH and pure water; cell durability during dry cathode operation.

References

1. Hydrogen Council, Path to hydrogen competitiveness: A cost perspecitve. 2020.
2. Hydrogen Europe. Hydrogen applications. https://hydrogeneurope.eu/hydrogen-applications (accessed Jan 7).
3. van Renssen, S. The hydrogen solution? *Nat. Clim. Change.* **2020,** *10* (9), 799-801.
4. de Coninck, H.; Revi, A.; Babiker, M.; Bertoldi, P.; Buckeridge, M.; Cargtwright, A.; Dong, W.; Ford, J.; Fuss, S.; Hourcade, J.-C.; Ley, D.; Mechler, R.; Newman, P.; Revokatova, A.; Shchultz, S.; Steg, L.; Sugiyama, T., Strengthening and implementing the global response. In *Global warming of 1.5°C. An IPCC special report on the impacts of global warming of 1.5°C above pre-industrial levels and related global greenhouse gas emission pathways, in the context of strengthening the global response to the threat of climate change, sustainable development, and efforts to eradicate poverty*, 2018.
5. IEA *The future of hydrogen*; IEA: Paris, 2019.
6. Ayers, K. Gigawatt-scale renewable hydrogen via water splitting as a case study for collaboration: The need to connect fundamental and applied research to accelerate solutions. *MRS Energy Sustain.* **2017,** *4*, E11.

7. Ayers, K.; Danilovic, N.; Ouimet, R.; Carmo, M.; Pivovar, B.; Bornstein, M. Perspectives on low-temperature electrolysis and potential for renewable hydrogen at scale. *Annu. Rev. Chem. Biomol. Eng.* **2019,** *10* (1), 219-239.

8. Fan, J.; Willdorf-Cohen, S.; Schibli, E. M.; Paula, Z.; Li, W.; Skalski, T. J. G.; Sergeenko, A. T.; Hohenadel, A.; Frisken, B. J.; Magliocca, E.; Mustain, W. E.; Diesendruck, C. E.; Dekel, D. R.; Holdcroft, S. Poly(bis-arylimidazoliums) possessing high hydroxide ion exchange capacity and high alkaline stability. *Nat. Commun.* **2019,** *10* (1), 2306.

9. Huang, G.; Mandal, M.; Hassan, N. U.; Groenhout, K.; Dobbs, A.; Mustain, W. E.; Kohl, P. A. Ionomer optimization for water uptake and swelling in anion exchange membrane electrolyzer: Oxygen evolution electrode. *J. Electrochem. Soc.* **2020,** *167* (16), 164514.

10. Huang, G.; Mandal, M.; Hassan, N. U.; Groenhout, K.; Dobbs, A.; Mustain, W. E.; Kohl, P. A. Ionomer optimization for water uptake and swelling in anion exchange membrane electrolyzer: Hydrogen evolution electrode. *J. Electrochem. Soc.* **2021,** *168* (2), 024503.

11. Bernt, M.; Gasteiger, H. A. Influence of ionomer content in IrO_2/TiO_2 electrodes on PEM water electrolyzer performance. *J. Electrochem. Soc.* **2016,** *163* (11), F3179-F3189.

12. Henkensmeier, D.; Najibah, M.; Harms, C.; Žitka, J.; Hnát, J.; Bouzek, K. Overview: State-of-the art commercial membranes for anion exchange membrane water electrolysis. *J. Electrochem. Energy.* **2020,** *18* (2), 024001-0240018.

13. Vincent, I.; Bessarabov, D. Low cost hydrogen production by anion exchange membrane electrolysis: A review. *Renew. Sust. Energ. Rev.* **2018,** *81*, 1690-1704.

14. Miller, H. A.; Bouzek, K.; Hnat, J.; Loos, S.; Bernäcker, C. I.; Weißgärber, T.; Röntzsch, L.; Meier-Haack, J. Green hydrogen from anion exchange membrane water electrolysis: A

review of recent developments in critical materials and operating conditions. *Sustain. Energ. Fuels.* **2020,** *4* (5), 2114-2133.

15. Leng, Y.; Chen, G.; Mendoza, A. J.; Tighe, T. B.; Hickner, M. A.; Wang, C.-Y. Solid-state water electrolysis with an alkaline membrane. *J. Am. Chem. Soc.* **2012,** *134* (22), 9054-9057.

16. Li, D.; Park Eun, J.; Zhu, W.; Shi, Q.; Zhou, Y.; Tian, H.; Lin, Y.; Serov, A.; Zulevi, B.; Baca Ehren, D.; Fujimoto, C.; Chung Hoon, T.; Kim Yu, S. Highly quaternized polystyrene ionomers for high performance anion exchange membrane water electrolysers. *Nat. Energ.* **2020,** *5*, 378-385.

17. Soni, R.; Miyanishi, S.; Kuroki, H.; Yamaguchi, T. Pure water solid alkaline water electrolyzer using fully aromatic and high-molecular-weight poly(fluorene-alt-tetrafluorophenylene)-trimethyl ammonium anion exchange membranes and ionomers. *ACS Appl. Energy Mater.* **2020,** *4* (2), 1053-1058.

18. Xiao, J.; Oliveira, A. M.; Wang, L.; Zhao, Y.; Wang, T.; Wang, J.; Setzler, B. P.; Yan, Y. Water-fed hydroxide exchange membrane electrolyzer enabled by a fluoride-incorporated nickel–iron oxyhydroxide oxygen evolution electrode. *ACS Catal.* **2021,** *11* (1), 264-270.

19. Carmo, M.; Fritz, D. L.; Mergel, J.; Stolten, D. A comprehensive review on PEM water electrolysis. *Int. J. Hydrogen Energy* **2013,** *38* (12), 4901-4934.

20. Mayerhöfer, B.; McLaughlin, D.; Böhm, T.; Hegelheimer, M.; Seeberger, D.; Thiele, S. Bipolar membrane electrode assemblies for water electrolysis. *ACS Appl. Energy Mater.* **2020,** *3* (10), 9635-9644.

21. Oener, S. Z.; Foster, M. J.; Boettcher, S. W. Accelerating water dissociation in bipolar membranes and for electrocatalysis. *Science* **2020,** *369* (6507), 1099.

22. Oener, S. Z.; Twight, L. P.; Lindquist, G. A.; Boettcher, S. W. Thin cation-exchange layers enable high-current-density bipolar membrane electrolyzers via improved water transport. *ACS Energy Lett.* **2021,** *6* (1), 1-8.

23. Jhong, H.-R. M.; Brushett, F. R.; Kenis, P. J. A. The effects of catalyst layer deposition methodology on electrode performance. *Adv. Energy Mater.* **2013,** *3* (5), 589-599.

24. Lim, A.; Kim, H.-j.; Henkensmeier, D.; Jong Yoo, S.; Young Kim, J.; Young Lee, S.; Sung, Y.-E.; Jang, J. H.; Park, H. S. A study on electrode fabrication and operation variables affecting the performance of anion exchange membrane water electrolysis. *J. Ind. Eng. Chem.* **2019,** *76*, 410-418.

25. Schuler, T.; Ciccone, J. M.; Krentscher, B.; Marone, F.; Peter, C.; Schmidt, T. J.; Büchi, F. N. Hierarchically structured porous transport layers for polymer electrolyte water electrolysis. *Adv. Energy Mater.* **2020,** *10* (2), 1903216.

26. Lettenmeier, P.; Kolb, S.; Sata, N.; Fallisch, A.; Zielke, L.; Thiele, S.; Gago, A. S.; Friedrich, K. A. Comprehensive investigation of novel pore-graded gas diffusion layers for high-performance and cost-effective proton exchange membrane electrolyzers. *Energy Environ. Sci.* **2017,** *10* (12), 2521-2533.

27. Suermann, M.; Gimpel, T.; Bühre, L. V.; Schade, W.; Bensmann, B.; Hanke-Rauschenbach, R. Femtosecond laser-induced surface structuring of the porous transport layers in proton exchange membrane water electrolysis. *J. Mater. Chem. A.* **2020,** *8* (9), 4898-4910.

28. Ionomr. Ionomer hydrogen info sheet. https://ionomr.com/wp-content/uploads/2018/12/Ionomr-Hydrogen-Info-Sheet.pdf (accessed September 15, 2020).

29. Dioide Materials. Sustainion anion exchange membranes. https://dioxidematerials.com/technology/sustainion-membranes/ (accessed February 2, 2021).

30. Wang, J.; Zhao, Y.; Setzler, B. P.; Rojas-Carbonell, S.; Ben Yehuda, C.; Amel, A.; Page, M.; Wang, L.; Hu, K.; Shi, L.; Gottesfeld, S.; Xu, B.; Yan, Y. Poly(aryl piperidinium) membranes and ionomers for hydroxide exchange membrane fuel cells. *Nat. Energ.* **2019,** *4* (5), 392-398.

31. Li, D.; Motz, A. R.; Bae, C.; Fujimoto, C.; Yang, G.; Zhang, F.-Y.; Ayers, K. E.; Kim, Y. S. Durability of anion exchange membrane water electrolyzers. *Energy Environ. Sci.* **2021,** *14* (6), 3393-3419.

32. Epsztein, R.; Shaulsky, E.; Qin, M.; Elimelech, M. Activation behavior for ion permeation in ion-exchange membranes: Role of ion dehydration in selective transport. *J. Membr. Sci.* **2019,** *580*, 316-326.

33. Xu, Q.; Oener, S. Z.; Lindquist, G.; Jiang, H.; Li, C.; Boettcher, S. W. Integrated reference electrodes in anion-exchange-membrane electrolyzers: Impact of stainless-steel gas-diffusion layers and internal mechanical pressure. *ACS Energy Lett.* **2020,** *6* (2), 305-312.

34. Bock, R.; Karoliussen, H.; Seland, F.; Pollet, B. G.; Thomassen, M. S.; Holdcroft, S.; Burheim, O. S. Measuring the thermal conductivity of membrane and porous transport layer in proton and anion exchange membrane water electrolyzers for temperature distribution modeling. *Int. J. Hydrogen Energy* **2020,** *45* (2), 1236-1254.

35. Evans, C. E.; Noble, R. D.; Nazeri-Thompson, S.; Nazeri, B.; Koval, C. A. Role of conditioning on water uptake and hydraulic permeability of Nafion® membranes. *J. Membr. Sci.* **2006,** *279* (1), 521-528.

36. Peron, J.; Mani, A.; Zhao, X.; Edwards, D.; Adachi, M.; Soboleva, T.; Shi, Z.; Xie, Z.; Navessin, T.; Holdcroft, S. Properties of Nafion® NR-211 membranes for PEMFCs. *J. Membr. Sci.* **2010,** *356* (1), 44-51.

37. Bezmalinović, D.; Radošević, J.; Barbir, F. Initial conditioning of polymer electrolyte membrane fuel cell by temperature and potential cycling. *Acta Chim. Slov.* **2014,** *62* (1), 5.

38. Qi, Z.; Kaufman, A. Quick and effective activation of proton-exchange membrane fuel cells. *J. Power Sources* **2003,** *114* (1), 21-31.

39. Balogun, E.; Barnett, A. O.; Holdcroft, S. Cathode starvation as an accelerated conditioning procedure for perfluorosulfonic acid ionomer fuel cells. *J. Power Sources Advances* **2020,** *3*, 100012.

40. Zhegur-Khais, A.; Kubannek, F.; Krewer, U.; Dekel, D. R. Measuring the true hydroxide conductivity of anion exchange membranes. *J. Membr. Sci.* **2020,** *612*, 118461.

41. Lindquist, G. A.; Xu, Q.; Oener, S. Z.; Boettcher, S. W. Membrane electrolyzers for impure-water splitting. *Joule* **2020,** *4* (12), 2549-2561.

TOC Graphic:

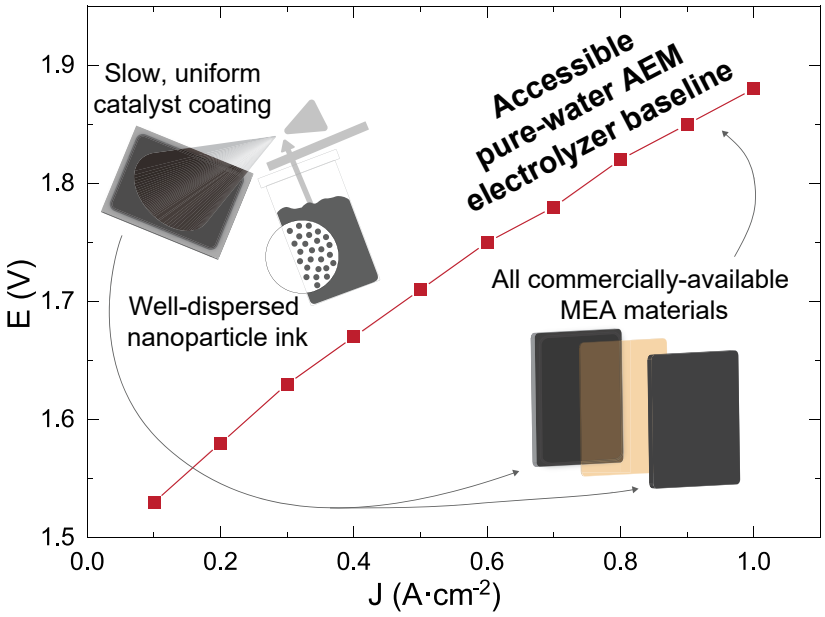
Slow, uniform
catalyst coating
Well-dispersed
nanoparticle ink
Accessible
pure-water AEM
electrolyzer baseline
All commercially-available
MEA materials
E (V)
J (A·cm-2)
1.5
1.6
1.7
1.8
1.9
0.0
0.2
0.4
0.6
0.8
1.0